

APPLICATION OF FRACTURE MECHANICS TO DESIGN OF SFRC TUNNEL LININGS AND DEVELOPMENT OF STRAIN-HARDENING CEMENTITIOUS COMPOSITES

H. Horii, P. Nanakorn and P. Kabele
Department of Civil Engineering, The University of Tokyo, Tokyo, Japan

Abstract

The application of fracture mechanics to the design of steel-fiber-reinforced concrete (SFRC) tunnel linings and the development of strain-hardening cementitious composites is presented. In the first part of the paper, a recently established design provision on the estimation of the load carrying capacity of SFRC tunnel linings is briefly introduced. The design method is based on the fracture mechanics of concrete. Existence of a crack and transmission of stress by fibers are considered in the estimation of the maximum resultant forces of the critical cross-section. In this study, the validity of the current design method is verified, and possible improvements of the design method are proposed. In the second part of the paper, we present an analytical model for fracture analysis of strain-hardening cementitious composites. Such an analytical tool is necessary for the evaluation of the performance of new materials used in structural members. Both multiple and localized cracking, which are characteristic of this class of materials, are represented in the model. A plasticity-based modeling

method is used for the distributed multiple cracking, while discrete modeling is employed for the localized cracks. Fracture tests of pseudo strain-hardening cement-based composites are analyzed, and predicted fracture energy is compared with reported experimental results.

1 Introduction

The fracture mechanics of concrete has been extensively studied for more than ten years in an effort to understand the fracture behavior of concrete under the application of loads. The governing mechanisms have been discovered especially for mode one crack growth phenomena. General agreement on governing mechanisms, their modeling, material characterization and analysis methods has to some extent been attained. Studies on the fracture mechanics of concrete have now entered the second stage which includes tasks such as, establishment of the analysis tools for general behavior of concrete structures including tensile and compressive fracture phenomena, application of fracture mechanics for design practice, and development of new cementitious materials based on fracture mechanics and micromechanics.

The first part of this paper is devoted to the application of fracture mechanics to the design of steel-fiber-reinforced concrete (SFRC) tunnel linings. A recently established Japanese design provision for SFRC tunnel linings, which is based on the fracture mechanics of concrete, is briefly introduced, and points to be improved are shown. Finally, a modified design method is proposed. The second part of the paper is devoted to a new class of materials – pseudo strain-hardening cement-based composites. Noting that analytical modeling is an essential part of the development of new materials, we present a fracture mechanics-based model for the strain-hardening cementitious composites. The model is used to analyze the effect of fiber volume fraction and specimen size on fracture energy and the results are compared with reported experimental data.

2 Fracture mechanics-based design provision for SFRC tunnel linings

2.1 Introduction

In the design of concrete linings, one of the limit states is the failure of a section after initiation and propagation of a crack. An increase in maximum resultant forces and greater toughness after the peak load are

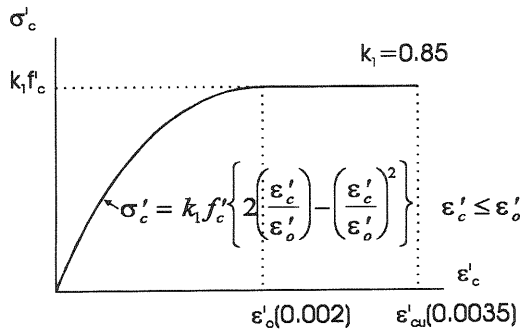


Fig. 1 Uniaxial compressive stress-strain curve

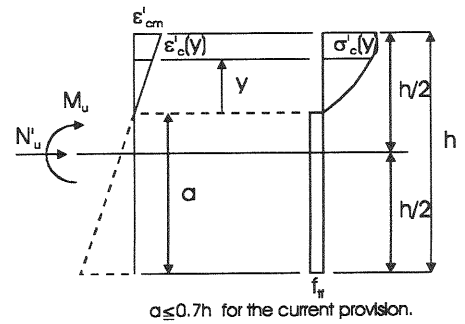


Fig. 2 Estimation method for sectional force capacity

expected in linings with SFRC, due to stress transmission across crack surfaces by fibers. To reflect such benefits of steel fibers in design, the design provision must take this stress transmission into account. This implies that a new design method is required to replace the conventional method, which ignores resistance to tensile stress. Knowledge of fracture mechanics is applied since the limit state is governed by the growth of a crack and stress transmission across it.

In 1992, “Recommendation for Design and Construction of Extruded Concrete Lining Method” was completed by Japan Railway Construction Public Corporation (1992). This is a design recommendation that is based on fracture mechanics. The main assumptions in the evaluation of the sectional capacity are as follows: axial strain in compression is proportional to the distance from the neutral axis, stress-strain curve in compression for SFRC members follows Fig. 1, tensile strength carried by fibers f_{tf} is considered for the tensile stress in SFRC members, and the maximum length of a crack is 70% of the thickness of the lining.

Fig. 2 shows the stress distribution used in the evaluation of the sectional capacity in the current design provision. The design method is based on the results of experiments. Even though the basic idea of fracture mechanics is employed through the introduction of the stress transmission along a crack, some assumptions are introduced, more or less, without clear supporting background. One of the points to be clarified would be the validity of the assumption of stress distribution. Constant stress, the tensile strength carried by fibers f_{tf} , is assumed along the crack. In reality, the transmitted stress decreases with increasing crack opening displacement. Another point to be investigated is the assumption of maximum crack length. The estimated bending moment capacity is larger with longer crack length.

It is specified that the tensile strength carried by fibers f_{tf} is to be determined from a bending test. However, if the same stress distribution is employed, the fiber stress f_{tf} determined from a small bending specimen overestimates the bending moment capacity of the lining with larger thickness. Although, in the current design provision, a factor for the member size is introduced, the magnitude of the factor is determined without theoretical support. It is desirable to identify the source of the size effect and to develop a design method without unclear factors.

2.2 Crack growth analysis of the critical section

2.2.1 Numerical analysis of the critical section

Instead of carrying out experiments and measurements of the critical sections of SFRC tunnel linings, we solve the problem shown in Fig. 3 by FEM analysis. It is a plane strain problem under bending moment and axial compressive force. The unit thickness of the specimen is considered for all calculations. Horii and Nanakorn (1993) show that consideration of a single crack at the critical section is sufficient even if there are distributed cracks at the initial stage. Therefore, only a single crack at the middle of the specimen is considered in the calculations. The propagation of the crack is captured by a cracked element which is an element with embedded displacement discontinuity (Nanakorn and Horii [1995]). The height of the sample is equal to the thickness of the lining. The length of the sample should be long enough to enclose the zone disturbed by the failure surface. Horii and Nanakorn (1993) show that the length of a square sample is sufficient. Thus, a square specimen is used in all analyses. The tension-softening curve used in the computation is approximated by a linear curve (see Fig. 4). The real tension-softening curve of SFRC usually contains a sharp-drop part at the beginning of the curve which can be neglected

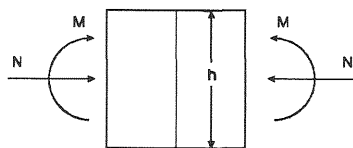


Fig. 3 Numerical analysis of the critical section

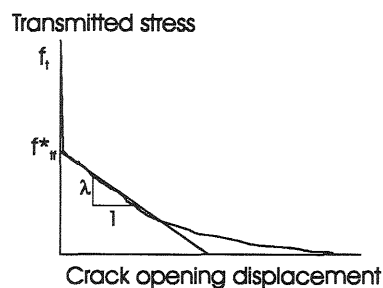


Fig. 4. Linear tension-softening curve

(Nanakorn [1993]). After the sharp drop, the tension-softening curve has quite a gentle slope. Therefore, it can be reasonably represented by a linear tension-softening relationship. Note that f_{ff}^* represents the stress after the sharp drop in the real tension-softening curve, and the slope of the linear curve is denoted by λ (see Fig. 4). For the nonlinearity in compression, a Drucker-Prager type constitutive equation with the same uniaxial stress-strain curve as the current design provision is employed (see Fig. 1).

2.2.2 Stress distribution in samples with different sizes

For the investigation, samples with heights of 150 mm, 200 mm, 300 mm and 400 mm, are solved. The axial stress distributions from FEM analysis along the critical cross-section at peak loads for all problems are plotted in Fig. 5. It is noticed that the transmitted tensile stresses in all cases look almost the same and are almost constant along their cracks. The crack lengths at the peak loads, on the other hand, are different in every case. The difference is expected to be greater when the slope of the tension-softening curve is steeper or, in another word, when the bridging by fibers is weaker and the material behavior is closer to that of plain concrete.

2.2.3 Stress distribution in samples with different slopes of tension-softening curves

Here, the effect of the slope of the tension-softening curve on the stress distribution at the peak load is investigated. The slope of the linear tension-softening curve is varied inside the reasonable range for SFRC. The obtained stress distributions at the peak loads are plotted in Fig. 6. It is

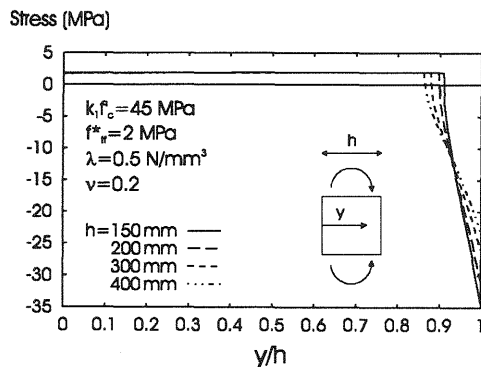


Fig. 5 Stress distribution along the critical section of samples with different sizes

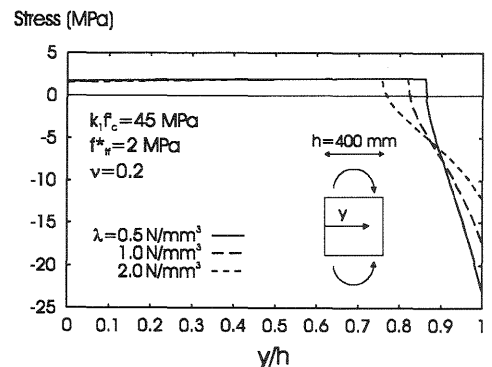


Fig. 6 Stress distribution along the critical section of samples with different λ

expected that the reduction of transmitted stress is remarkable when the slope of the tension-softening curve is steeper. However, in SFRC with λ less than 2 N/mm^3 , such a significant reduction in the transmitted stress is not observed in a pure bending case, as shown in Fig. 6. The effect of the slope of the tension-softening curve is dominant in the crack length at the peak load. The crack length at the peak load decreases with steeper slope of the tension-softening curve.

2.3 Proposal for a design method

2.3.1 Determination of the tensile strength carried by fibers

Judging from the results of the previous section, we find that it is reasonable to adopt the assumption of constant transmitted tensile stress along the crack; this is the assumption employed in the current design provision. In this section, we propose a method to determine the tensile strength carried by fibers f_{tf} from the bending test of a small sample. Consider the design stress distribution shown in Fig. 2. The stress-strain relationship in compressive zone follows the stress-strain relationship in Fig. 1. The sectional forces can be written as

$$\begin{aligned}
 N' / b &= \int_0^{h-a} \sigma'_c(y) dy - \sigma_{yf} a \quad , \\
 M / b &= \int_0^{h-a} \sigma'_c(y) \left(y + a - \frac{h}{2} \right) dy + \sigma_{yf} a \left(\frac{h}{2} - \frac{a}{2} \right)
 \end{aligned}
 \tag{1}$$

where b is the width of the sample and σ_{yf} is the tensile stress carried by fibers which is constant along the crack.

Employing the assumption that the axial strain beyond cracking region is proportional to the distance from the neutral axis, we obtain

$$\epsilon'_c = \frac{\epsilon'_{cm}}{h-a} y
 \tag{2}$$

where ϵ'_{cm} is the compressive strain at the top of the section.

From Eqns 1 and 2 and given values of ϵ'_{cm} , N' and M , one can calculate the tensile stress carried by fibers σ_{yf} and the crack length a . To check the validity of this stress distribution, σ_{yf} and a are estimated by using Eqns 1 and 2 for any given M and its corresponding ϵ'_{cm} from FEM

analysis. The obtained crack length a is then compared with the crack length obtained from FEM analysis. As a result, good agreement is found. Therefore, it can be concluded that the assumed stress distribution is reasonable.

Employing the same method, we calculate σ_f for the heights of 150 mm and 400 mm, and the obtained σ_f is plotted in Fig. 7 with respect to the crack mouth opening displacement (CMOD) from FEM. From the figure, it is noticed that σ_f decreases when CMOD increases, and σ_f for both cases is almost the same for the same CMOD. From the experiments of small beams, it is difficult to identify the peak load to be used for the determination of the tensile strength carried by fibers, f_{ff} , because the load-displacement curves obtained in actual tests scatter a lot. Therefore, instead of peak, σ_f at a specific CMOD is used as the tensile strength carried by fibers, f_{ff} . From experimental observation, it is found that CMOD at peak is usually less than 1.5 mm for SFRC. Thus, it is safe to use 1.5 mm as a reference. The rate of reduction of σ_f with increasing CMOD is larger when the tension-softening curve is steeper, i.e., fiber bridging is of less quality. Therefore, this method assures the quality of fiber bridging, since f_{ff} is very small for poor fiber bridging.

To determine f_{ff} , one carries out the bending test on a small specimen and measures the axial strain at the top of the critical section and the applied moment when CMOD is equal to 1.5 mm. From ϵ'_{cm} and M , f_{ff} is calculated from Eqns 1 and 2. In the existing design provision, f_{ff} is also recommended to be determined from the bending test. With maximum moment obtained from the test and the assumption that maximum crack length is equal to 70% of the thickness, f_{ff} is calculated. However, it is observed that the critical crack length for SFRC members is usually longer than 70% of the thickness. Hence, limiting crack length to 70% of the thickness leads to an overestimation of f_{ff} .

2.3.2 Prediction of sectional capacity

After f_{ff} is obtained, we use it to predict the maximum sectional force capacity of the lining with different thickness. In the prediction, the same stress distribution shown in Fig. 2 is employed. The maximum bending moment M_u for a given value of N'_u for sections with different thickness is obtained from Eqns 1 and 2. At this time, however, the crack length at the peak load is required. This is expected to be provided in the design provision. As it is seen in Fig. 5 and Fig. 6, the crack length at peak load

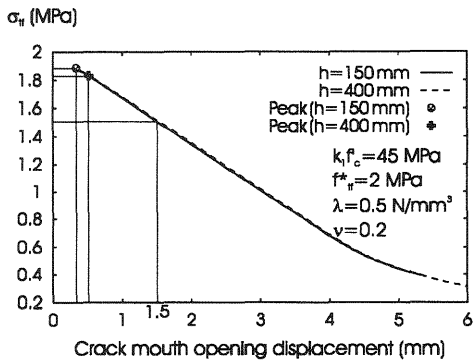


Fig. 7 Approximation of f_{tf} from a small specimen

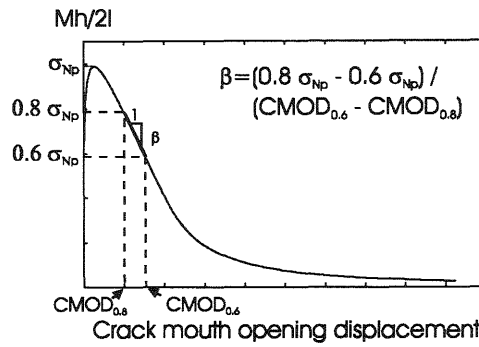


Fig. 8 Definition of β

varies with respect to the size of the specimen and the slope of the tension-softening curve. It means that the crack length must be a function of the lining thickness h and the slope of the tension-softening curve λ . In order to select the appropriate crack length, the slope of the tension-softening curve must be known.

It is not practical to obtain the slope of the tension-softening curve directly from a direct tension test because the test is difficult and requires a sophisticated machine. Therefore, a method to estimate the slope of the tension-softening curve from the bending test is proposed. It is noticed that the post-peak slope of the moment-CMOD curve has a unique relationship with the slope of the tension-softening curve. This means that the slope of the tension-softening curve can be estimated from the post-peak slope of the moment-CMOD curve. In this study, the post-peak slope of the moment-CMOD curve, β , is defined in Fig. 8 where normalized moment is used. Even if it is difficult to identify peak, the error will not affect the value of β much because the post-peak slope is usually almost linear.

In this new design method, one obtains f_{tf} and β from the bending test of a small beam. From β and the thickness of the lining, an appropriate crack length will be obtained from a table provided in the design provision. A table can be prepared because the relationship between β and λ is unique, and the appropriate crack length is a function of λ and the thickness of the lining. Using that crack length and f_{tf} , the sectional capacity can finally be calculated. It is important to note that, in all cases, the top compressive strain must not be greater than the ultimate compressive strain ϵ'_{cu} . When the maximum compressive strain reaches the ultimate compressive strain, the failure mode is understood to change into the compression failure, and the crack length can be less than the value given in the design table. Fig. 9

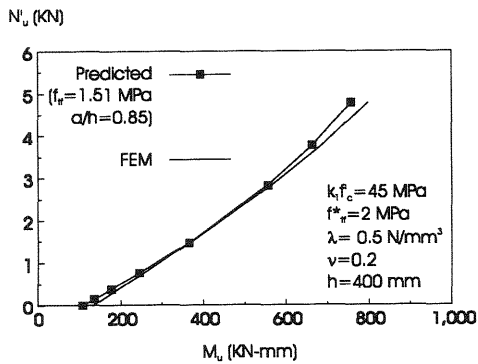


Fig. 9 Interaction diagram with $\lambda=0.5 \text{ N/mm}^3$

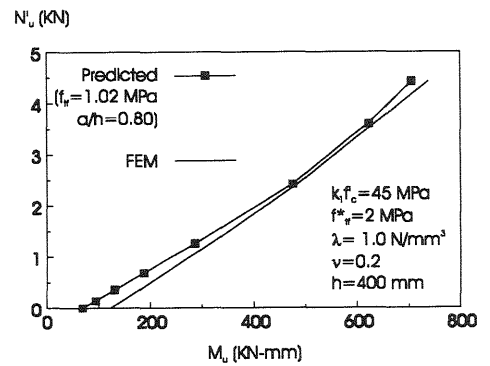


Fig. 10 Interaction diagram with $\lambda=1.0 \text{ N/mm}^3$

and Fig. 10 show the prediction of the capacity for the section of 400 mm height. The crack lengths used in the prediction are determined in such a way that good estimation for each different λ is obtained.

3 Modeling and analysis of strain-hardening cementitious composites

3.1 Introduction

The previous section shows an example of the research of the cement-based composites that has already entered the phase of engineering application involving development of a design method. Meanwhile, a great effort has been being spent on development of new materials with even more enhanced properties. A group of such materials, called engineered cementitious composites (ECCs), has been recently developed by Li and co-workers (Li [1993], Li and Hashida [1992]).

The ECCs belong to a class of cementitious composites reinforced with short randomly distributed and randomly oriented fibers. The ECCs distinguish themselves by such features as ability to exhibit pseudo strain-hardening behavior under tensile and shear loads, and a fracture energy and strain capacity as much as two orders of magnitude higher than those of conventional cement-based materials. These superior properties are attained by means of a tailored micromechanical structure, which provides the composites with ability to undergo multiple cracking distributed over a large volume of material prior to formation of a localized crack.

The ECCs have been a subject of both experimental (e.g., Li and Hashida [1992], Li et al. [1994], Maalej et al. [1994]) and theoretical (e.g., Li [1992]) research, but little attention has been paid to analytical modeling and computer simulation of their behavior. The importance of the computer

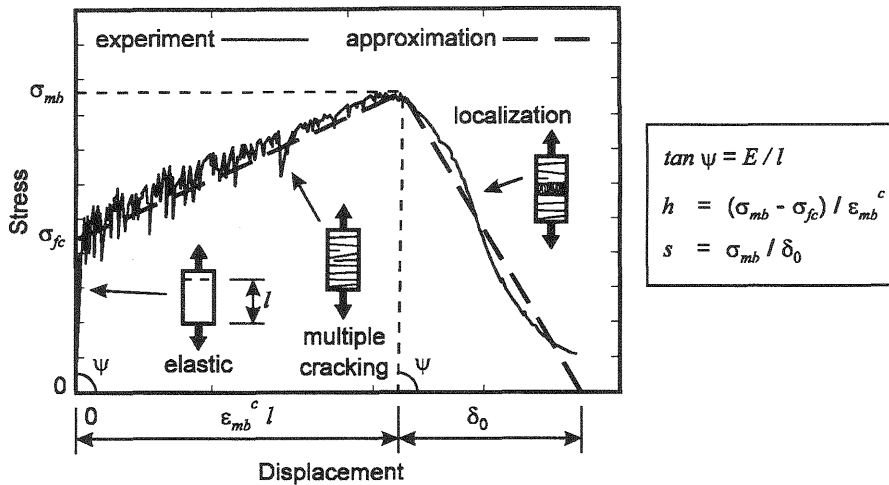


Fig. 11 Typical uniaxial stress-displacement curve of ECC

simulation in material development lies in the fact that it can be used to investigate the performance of structural members in which the developed material is used.

In light of this background, our group have developed an analytical model for ECCs. As the fracture behavior dominates the ECCs' response to applied loads, the model emphasizes representation of both the multiple cracking and the localized cracking.

3.2 Analytical model for ECCs

3.2.1 Fracture behavior of ECCs

In order to construct an adequate model for the ECCs, first we have to identify the dominant mechanism of their mechanical behavior. We construct the analytical model based on the experimental results reported by Maalej et al. (1994) and Li et al. (1994).

Due to the short fiber lengths and random fiber distribution and orientation, the ECCs can be considered as macroscopically homogenous and isotropic materials. The hardening behavior of ECCs is associated with the multiple cracking, which takes place in the form of closely spaced microcracks oriented more or less at the right angle to the direction of the maximum principal stress. When the width of some of the multiple cracks exceeds certain critical level, this crack starts to follow a softening regime and the fracture becomes localized into this crack.

Fig. 11 shows an example of a uniaxial stress-displacement curve of an ECC consisting of cement paste reinforced with 2% by volume of

polyethylene fibers. The two distinct types of cracking are also indicated in the figure.

As the nature of the multiple and localized cracking is different we use different modeling methods for the two types of cracking.

3.2.2 Modeling of the multiple cracking

As the multiple cracking is characterized by high crack density and small crack widths, discrete representation of each crack would not be practical. Instead, we model the composite in the multiple cracking state as a continuous material with an additional strain (cracking strain) that represents the crack opening displacements and crack density. The model must reflect the following characteristics of the multiple cracking:

- the material in the multiple cracking state exhibits overall strain-hardening,
- the deformation due to the multiple cracking is inelastic,
- the multiple cracking induces an anisotropy to the material.

Accordingly, we use the incremental theory of plasticity to represent the effect of the multiple cracking. We employ the Rankine yield function which is given for a 2-D stress state in the following form:

$$F \equiv \frac{\sigma_{xx}^* + \sigma_{yy}^*}{2} + \sqrt{\left(\frac{\sigma_{xx}^* - \sigma_{yy}^*}{2}\right)^2 + \left(\frac{\sigma_{xy}^* + \sigma_{yx}^*}{2}\right)^2} - \sigma_{fc} = 0 \quad (3)$$

where σ_{fc} is the first crack strength and σ_{xx}^* , σ_{yy}^* , σ_{xy}^* and σ_{yx}^* are defined by the kinematic hardening rule as follows:

$$\sigma_i^* = \sigma_i - \alpha_i \quad (4)$$

Here i equals successively to xx , yy , xy and yx . Then σ_i is a vector consisting of in-plane components of the stress tensor. The vector α_i is defined as:

$$d\alpha_i = h d\epsilon_i^c \quad (5)$$

in which $d\epsilon_i^c$ is the incremental cracking strain vector and h is a material parameter that reflects the hardening behavior.

The yield function defined by Eqn 3 and the associated flow rule are used in order to represent the fact that the multiple cracking is initiated on planes normal to the maximum principal stress when its magnitude reaches the first crack strength. It is shown by Kabele and Horii (1995) that the present modeling concept implies that at any location the multiple cracking can occur in an infinite number of directions, depending on the direction of the principal stress. The kinematic hardening rule (Eqns 4 and 5) then reflects the assumption that the initiation and response of any set of multiple cracks oriented in certain direction is affected neither by the normal stress acting in direction parallel to the cracks nor by the multiple cracking in perpendicular direction.

The material parameters h and σ_{fc} are determined from the uniaxial stress-displacement curve, as shown in Fig. 11. It is also seen in Fig. 11 that the hardening portion of the stress-displacement curve is almost linear, which allows us to use constant h .

3.2.3 Modeling of the localized cracks

The direction of the maximum principal cracking strain is normal to the direction of the most developed multiple cracks. We define the condition for initiation of the localized cracking so that the localized crack forms on a plane normal to the direction of the maximum principal cracking strain when its magnitude reaches a critical level denoted as ε_{mb}^c .

The localized cracks are characterized by large widths, low density and presence of bridging. The localized cracks are modeled as discrete discontinuities in the displacement field with the effect of the bridging being represented by a traction applied to the crack surfaces. Generally, both normal and tangent components of the transmitted traction are related to the relative displacements of the crack surfaces. However, for a lack of experimental data we assume that the normal component of the transmitted traction decreases depending only on the normal COD, while the tangent traction stays constant. The normal traction to normal COD relationship, known as the tension-softening relationship, is given in an incremental form as:

$$dt_n = s d\delta_n \quad (6)$$

where dt_n stands for the incremental normal traction, s is the slope of the tension softening curve, and $d\delta_n$ is the incremental normal COD.

The localized crack model is defined by the critical cracking strain ε_{mb}^c and the tension-softening curve. It is seen in Fig. 11 that the value of ε_{mb}^c is determined from the result of the uniaxial tension test. The figure also shows that as the descending part of the uniaxial stress-displacement curve is almost linear, we set the value of the parameter s constant.

3.2.4 Implementation and verification

The plasticity-based model for the multiple cracking is implemented into an FEM program by means of the incremental constitutive law. For the localized crack model we employ the cracked element developed by Nanakorn and Horii (1995). As all the governing equations are given in an incremental form, an algorithm based on the Euler method is used to integrate the incremental solutions.

The validity of the analytical model has been verified by Kabele and Horii (1995), who used it to solve several examples involving double cantilever beam specimens and compared the results with experimental data. They found that although the model tended to overestimate the specimen ultimate strength, it essentially captured all major features of the ECCs, such as, the trend of the load-displacement curve and existence, direction and extent of both the multiple cracking and the localized cracking.

3.3 Analysis of fracture tests and prediction of fracture energy

3.3.1 Analysis of the effect of fiber volume fraction on the fracture energy
Maalej et al. (1994) experimentally studied the aspects of energy dissipation in ECCs. The authors considered that the total fracture energy of the composite J_c , which is defined as the energy dissipated by unit area growth of the stress free crack, consists of two components: the fracture energy contributed by development of the multiple cracking zone (denoted as J_m), and the fracture energy contributed by propagation of the localized crack with bridging (denoted as J_b). A J-integral-based technique was used in the experimental study to measure the fracture energy and its components.

The bridging fracture energy J_b was evaluated by integrating the post-peak part of the stress-displacement curve obtained from a uniaxial tension test. In order to evaluate the total fracture energy J_c , two double cantilever beam (DCB) specimens were tested. The two specimens were identical except for a slight difference in the initial notch length. The total fracture

Table 1 Material parameters of ECCs with different V_f

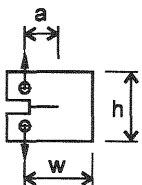
V_f (%)	E (GPa)	ν (-)	σ_{fc} (MPa)	ϵ_{mb}^c (%)	σ_{mb} (MPa)	δ_0 (mm)
0.8	10	0.2	2.0	2.27	2.85	6.27
1.0	10	0.2	2.0	2.82	3.05	6.17
2.0	22	0.2	2.2	5.78	4.32	6.62
3.0	10	0.2	2.5	6.15	4.97	5.28

energy was calculated as the area enclosed between the two specimens' load-displacement curves divided by the initial notch length difference and the specimen thickness. The value of J_m was then calculated as a difference between J_c and J_b .

Using the method described above, we tried to reproduce analytically the effect of the fiber volume fraction on the fracture energy that was reported in the experimental study by Maalej et al. (1994). The analyses were carried out for an ECC consisting of cement paste reinforced by polyethylene fibers. Four composites with different fiber volume fractions V_f (0.8%, 1%, 2% and 3%) were examined. The material parameters for each composite were determined from its respective uniaxial stress-displacement curve provided by Li (1994). The parameters are listed in Table 1. The dimensions of the analyzed DCB specimens were identical with those used in the experimental study, that is, a medium size DCB was used for V_f equal to 0.8% and 1% and a large size DCB was used for V_f equal to 2% and 3%. The specific dimensions of each specimen are listed in Table 2.

Fig. 12 shows the analytical results plotted together with the experimental results reported by Maalej et al. (1994). It is seen that although the analytical model tends to overestimate the fracture energy, it correctly reproduces the trend that with increasing fiber volume fraction the fracture energy initially increases but later becomes saturated. The overestimation of the fracture energy might be attributed to the fact that the material parameters for each volume fraction were determined from a limited amount of experimental data. Hence a large error might have been involved.

Table 2 Dimensions of the DCB specimens



size	h (cm)	w (cm)	a_1 (cm)	a_2 (cm)
small	15.3	12.7	6.5	7.4
medium	30.0	31.0	11.7	14.7
large	58.5	49.0	13.4	21.5

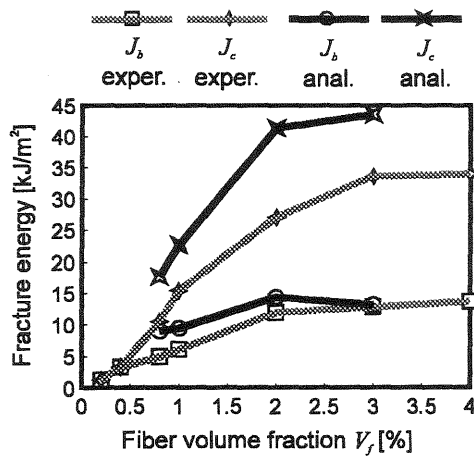


Fig. 12 Effect of fiber volume fraction on fracture energy

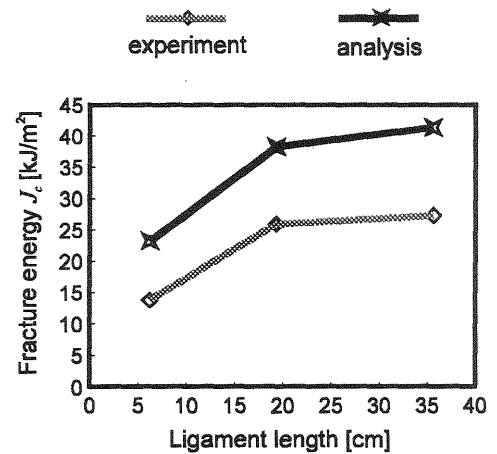


Fig. 13 Effect of specimen size on fracture energy

3.3.2 Analysis of the effect of specimen size on the fracture energy
 Maalej et al. (1994) also observed that for a constant fiber volume fraction, specimens of different sizes yielded different values of the fracture energy. Specifically, smaller specimens exhibited smaller fracture energy. The reason was that the development of the multiple cracking zone was constrained by proximity of boundaries in the smaller specimens, which resulted in less energy dissipation.

We tried to reproduce analytically this phenomenon. Using the same technique as in the previous analyses we computed the values of the fracture energy for DCB specimens of three different sizes (see Table 2). The material used in all of these analyses was the polyethylene fiber reinforced cement paste with fiber volume fraction equal to 2%.

Fig. 13 compares the analytical results with the experimental results reported by Maalej et al. (1994). It is seen that the analysis correctly reproduced the fact that the small specimen gave the value of the fracture energy almost fifty percent lower than the large one. Also in both experiment and analysis, the fracture energy of the medium size specimen was not much different from the one of the large specimen.

3.4 Concluding remarks

A fracture mechanics-based analytical model has been used to analyze fracture tests of ECC specimens. The results confirm capability of the present model to predict the fracture behavior of the ECCs, such as, the effect of the fiber volume fraction and the specimen size on the fracture energy.

4 Acknowledgment

The authors are thankful to Professor Victor C. Li for providing his helpful advice and for supplying the experimental data.

5 References

- Horii, H. and Nanakorn, P. (1993) Fracture mechanics based design of SFRC tunnel lining, in **Size Effect in Concrete Structures** (eds H. Mihashi, H. Okamura and Z.P. Bazant), E&FN Spon, London, 429-440.
- Japan Railway Construction Public Corporation (1992) **Recommendation for Design and Construction of Extruded Concrete Lining Method**. Yoshii Shoten, Tokyo (in Japanese).
- Kabele, P. and Horii, H. (1995) Analytical model for fracture analysis of pseudo strain-hardening cementitious composites, submitted to **Proc. of Japan Soc. of Civ. Eng.**
- Li, V.C. (1992) Postcrack scaling relations for fiber reinforced cementitious composites. **J. of Mat. in Civ. Eng.**, Vol. 4, No. 1, 41-57.
- Li, V.C. (1993) From micromechanics to structural engineering – the design of cementitious composites for civil engineering applications. **Proc. of Japan Soc. of Civ. Eng.**, No. 471/1-24, 37-48.
- Li, V.C. (1994) Personal communication.
- Li, V.C. and Hashida, T. (1992) Ductile fracture in cementitious materials?, in **Fracture Mechanics of Concrete** (ed Z.P. Bazant), Elsevier Applied Science, London and New York, 526-535.
- Li, V.C. et al. (1994) On the shear behavior of engineered cementitious composites. **Advn. Cem. Bas. Mat.**, 1, 142-149.
- Maalej, M. et al. (1994) **Effect of Fiber Volume Fraction on the Off-Crack-Plane Fracture Energy in Strain Hardening Engineered Cementitious Composites**. UMCEE Report No. 94-4, University of Michigan, Ann Arbor.
- Nanakorn, P. (1993) **Fracture Mechanics Based Design Method of SFRC Tunnel Lining**. Doctoral Dissertation, The University of Tokyo, Japan.
- Nanakorn, P. and Horii, H. (1995) A finite element with embedded displacement discontinuity, will appear in **Proc. of EASEC-5**, Queensland, Australia.